https://dx.doi.org/10.21577/0103-5053.20210161

J. Braz. Chem. Soc., Vol. 33, No. 5, 425-436, 2022
©2022 Sociedade Brasileira de Química

Article

Temperature Dependent Emission Properties of Re^{I} Tricarbonyl Complexes with Dipyrido-Quinoxaline and Phenazine Ligands

Cristiane L. Ramos,[a] Fernando S. Prado,[a] Marcos Eduardo G. Carmo,[a] Giliandro Farias,[b] Bernardo Souza,[b] Antonio Eduardo H. Machado[a,c] and Antonio Otavio T. Patrocinio*[,a]

[a]*Laboratório de Fotoquímica e Ciência de Materiais, Instituto de Química, Universidade Federal de Uberlândia, 38400-902 Uberlândia-MG, Brazil*

[b]*Departamento de Química, Universidade Federal de Santa Catarina, 88040-900 Florianópolis-SC, Brazil*

[c]*Programa de Pós-Graduação em Ciências Exatas e Tecnológicas, Unidade Acadêmica Especial de Física, Universidade Federal de Catalão, 75705-220 Catalão-GO, Brazil*

In this work, the emission properties of *fac*-[Re(CO)$_3$(NN)(py)]$^+$, NN = 1,10-phenanthroline (phen), dipyrido[3,2-*f*:2',3'-*h*]quinoxaline (dpq) and dipyrido[3,2-*a*:2'3'-*c*]phenazine (dppz); py = pyridine were investigated in different temperatures, ranging from 80 to 300 K, and in different solvent mixtures and in polymethyl methacrylate. The changes observed in the emission quantum yields were rationalized based on a two-level excited state model, in which the non-emissive upper state is thermally populated and decays faster than the lowest lying emissive state. *fac*-[Re(CO)$_3$(dpq)(py)]$^+$ is a metal-to-ligand charge transfer (MLCT) emitter as the complex with phen but exhibits smaller emission quantum yields, being more sensitive to the solvent. This behavior was rationalized by quantum-mechanical calculations including the spin-orbit coupling matrix elements, revealing that intersystem crossing from the lowest singlet excited state in *fac*-[Re(CO)$_3$(dpq)(py)]$^+$ likely occurs to triplet states lying at higher energies. Similar behavior were observed for *fac*-[Re(CO)$_3$(dppz)(py)]$^+$, although the later exhibits intraligand emission that are strongly quenched in fluid solutions by low-lying MLCT states. The fundamental studies carried out here provide new insights on the excited state dynamics of Re^{I} complexes with dipyrido-quinoxaline and phenazine ligands and can contribute for further advances on their application as luminescent probes.

Keywords: luminescence, photophysics, spin-orbit coupling, rhenium complexes

Introduction

The emissive properties of Re^{I} polypyridyl complexes have called growing attention due their highly modularity in terms of the ligands employed and the surrounding media.[1-4] Such properties have been successfully applied in the development of light-emissive devices (LEDs), biomarkers, ion sensors, among other technological applications.[5-8] In fluid solution and in biological environments, the typical long-lived emitting states of Re^{I} polypyridyl complex have been consistently employed as specific biological probes,[9-12] and for sensing of molecular oxygen and other triplet ground state molecules.[13-15] In more constrained media such as in polymeric matrixes,[16-19] variable photophysical behavior is observed as a function of the ligand structure and the specific linkage with the matrix. This flexibility has found interesting applications in LEDs.[20,21]

The useful photochemical and photophysical properties of these complexes arise from different classes of excited states, including metal-to-ligand charge transfer (MLCT), ligand-to-ligand charge transfer (LLCT), ligand-to-metal charge-transfer (LMCT), intraligand (IL) and metal-centered (MC) states, which the dynamics have been object of detailed experimental and theoretical studies.[1,22-25] Among the different polypyridyl

*e-mail: otaviopatrocinio@ufu.br
Editor handled this article: Jaísa Fernandes Soares

ligands employed in rhenium(I) complexes, pyrazino [2,3-*f*][1,10]phenanthroline derivatives such as dipyrido[3,2-*a*:2'3'-*c*]phenazine (dppz) and dipyrido[3,2-*f*:2',3'-*h*]quinoxaline (dpq) have called special attention due their rich photophysical behavior. Rhenium(I) complexes with the dppz ligand have been successfully applied as light-switch deoxyribonucleic acid (DNA) probes,[26-32] while complexes with dpq have been explored as avidin probes.[33-35]

Despite the photophysics and excited state dynamics of such complexes are well reported, especially those employing dppz as polypyridyl ligand, there are still open questions about the interconversion among the different singlet and triplet states during the relaxation process. Particularly, for complexes with dpq, no experimental or theoretical data can be found in the literature concerning the influence of temperature and medium rigidity on the excited state dynamics and, moreover no information about the role of upper-lying triplet states on the emission properties of such complexes is available. Aiming at a deeper understanding of the excited state dynamics in these Re^{I} complexes, herein we investigated the temperature-dependent emission properties of a series of Re^{I} complexes, *fac*-[Re(CO)$_3$(NN)(py)]$^+$, NN = 1,10-phenanthroline (phen), dpq or dppz; py = pyridine, Scheme 1. Along with experimental data, spin-orbit coupling (SOC) matrix elements between singlet and triplet excited states were computed using our previous reported methodology,[36,37] allowing for the description of differences in the excited state deactivation as a function of the polypyridyl ligand.

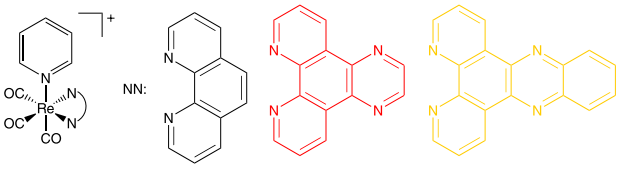

Scheme 1. Rhenium(I) tricarbonyl complexes investigated in this work.

Experimental

All solvents employed were high performance liquid chromatography (HPLC) grade. [ReCl(CO)$_5$], 1,10-phenantroline (phen), pyridine (py), trifluoromethanesulfonic acid, polymethyl methacrylate (PMMA) molecular weight (M$_w$) = 120000 and Rhodamine 6G were purchased from Aldrich (Darmstadt, Germany) and were used without further purification. The ligands, dipyrido [3,2-*f*:2',3'-*h*]quinoxaline (dpq) and dipyrido[3,2-*a*:2'3'-*c*] phenazine (dppz) were synthesized as described previously.[38-40] The *fac*-[Re(CO)$_3$(NN)(py)]PF$_6$ complexes, NN = phen (**1**), dpq (**2**) and dppz (**3**), were prepared following the procedures described earlier for similar complexes.[41] Product purity was confirmed by elementary analyses and ^{1}H nuclear magnetic resonance (NMR).

For *fac*-[Re(CO)$_3$(phen)(py)]PF$_6$ (**1**), yield was 87%; anal. calcd. for ReC$_{20}$H$_{13}$N$_3$O$_3$PF$_6$: C, 35.61%; N, 6.23%; H, 1.94%, found: C, 35.14%; N, 6.06%; H, 2.16%; ^{1}H NMR (400.1 MHz, CD$_3$CN) δ 10.36 (dd, 2H, *J* 1.32, 5.10 Hz), 9.59 (dd, 2H, *J* 1.36, 8.10 Hz), 9.02 (dd, 2H, *J* 1.48, 6.50 Hz), 8.92 (s, 2H), 8.87 (dd, 2H, *J* 5.12, 8.11 Hz), 8.50 (m, 1H), 7.94 (m, 2H).

For *fac*-[Re(CO)$_3$(dpq)(py)]PF$_6$ (**2**), yield was 92%; anal. calcd. for ReC$_{25}$H$_{22}$N$_5$O$_3$PF$_6$: C, 47.91%; N, 11.18%; H, 3.54%, found: C, 47.86%; N, 11.05%; H, 3.36%; ^{1}H NMR (400.1 MHz, CD$_3$CN) δ 10.54 (dd, 2H, *J* 1.24, 8.40 Hz), 10.44 (dd, 2H, *J* 1.48, 5.14 Hz), 9.95 (s, 2H), 9.06 (dd, 2H, *J* 1.40, 6.38 Hz), 9.01 (dd, 2H, *J* 5.40, 8.46 Hz), 8.50 (m, 1H), 7.96 (m, 2H).

For *fac*-[Re(CO)$_3$(dppz)(py)]PF$_6$ (**3**), yield was 79%; anal. calcd. for ReC$_{26}$H$_{15}$N$_5$O$_3$PF$_6$: C, 40.01%; N, 8.97%; H, 1.94%; found: C, 39.86%; N, 8.75%; H, 1.80%; ^{1}H NMR (400.1 MHz, CD$_3$CN) δ 10.66 (dd, 2H, *J* 1.36, 8.30 Hz), 10.42 (dd, 2H, *J* 1.32, 5.28 Hz), 9.22 (dd, 2H, *J* 3.36, 6.52 Hz), 9.11 (dd, 2H, *J* 1.52, 6.64 Hz), 9.02 (dd, 2H, *J* 5.28, 8.30 Hz), 8.89 (dd, 2H, *J* 3.20, 6.68 Hz), 8.52 (m, 1H), 7.99 (m, 2H).

Absorption spectra were recorded on a double beam Shimadzu UV-1650 spectrophotometer (Kyoto, Japan). ^{1}H NMR spectra were recorded on a DRX-400 MHz Bruker Ascend 400 (Leipzig, Germany) spectrometer using the residual solvent signal as internal standard. Elemental analysis was carried out in a PerkinElmer 2400 CHNS analyzer (Whaltam, USA). The measurements were recorded in a diamond crystal plate, using 16 scans at a resolution of 4 cm^{-1}.

Room temperature emission measurements were performed in argon degassed acetonitrile solutions in a 1.000 cm quartz cuvette. Emission quantum yields were determined taking the *fac*-[ClRe(CO)$_3$(phen)] complex as standard (ϕ_{em} = 0.018 in CH$_3$CN at 298 K).[42] Temperature dependent experiments were performed by coupling a Janis VNF-100 liquid nitrogen cryostat (Los Angeles, USA) to the spectrofluorometer. The samples were kept in a closed 0.1000 cm quartz cuvette placed at ca. 45° of the excitation beam. The sample chamber is surrounded by a jacket that was evacuated at 10^{-4} torr to reduce/eliminate moisture condensation. Temperature control was obtained with a Cryo-con 22C controller (Los Angeles, USA) connected to a built-in Si diode thermometer. Samples were kept at least 30 min at each temperature to ensure thermal equilibrium. The samples were dissolved in degassed 4:1 (v/v) ethanol/

methanol (EtOH/MeOH 4:1) or 5:4 (v/v) propionitrile/butyronitrile (prop/but 5:4) mixtures. Sample concentrations varied in the range of 2×10^{-4} to 5×10^{-4} mol L^{-1}.

PMMA films containing the investigated complexes were prepared by mixing 250 mg of PMMA (M_w = 120000) previously dissolved in acetonitrile with the respective complexes. The concentrations of the complexes were adjusted so the final film with thicknesses of ca. 2 mm exhibit absorbances in the range of 0.1-0.2 at 350 nm. Emission spectra at room temperature were recorded in the front surface excitation/emission geometry with the film surfaces at ca. 45º from the incident beam. Emission quantum yields in PMMA at 298 K were determined taking Rhodamine 6G as standard (ϕ_{em} = 0.75).[43]

Emission quantum yields at different temperatures (ϕ_{em}^T) were determined by the equation 1, following the procedure reported by Worl *et al.*[44] S_T and S_{298} are the respective emission band areas of the sample at a given temperature (T) and at 298 K. ϕ_{em}^{298} is the sample emission quantum yield at 298 K in the employed solvent. The reported values are averages of, at least, three independent experiments.

$$\phi_{em}^{T} = \phi_{em}^{298} \frac{S_T}{S_{298}} \quad (1)$$

Equation 1 is a simplification from equation 2, which considers the variation of the absorbance as a function of the temperature (A_{298}/A_T) and also the changes on the refractive index (η) of the solvent. The simplification follows from previous observation that, at 77 K, (A_{298}/A_T) decreases by ca. 16% and $(\eta_T/\eta_{298})^2$ increases by 15%[44,45] and leads to estimated uncertainties of ± 20%.

$$\phi_{em}^{T} = \phi_{em}^{298} \left(\frac{S_T}{S_{298}}\right)\left(\frac{A_{298}}{A_T}\right)\left(\frac{\eta_T}{\eta_{298}}\right)^2 \quad (2)$$

Theoretical methods employing density functional theory (DFT) and time-dependent (TD) DFT were carried out to obtain insights on the nature and energies of the frontiers orbitals. These calculations were carried out in Orca 4.2.1 software package[46] at DFT level using the PBE0.[47,48] The basis set for the rhenium(I) atom was SARC-ZORA-TZVP and, for the other atoms, ZORA-Def2-TZVP. The scalar-relativistic method ZORA was employed to account for relativistic effects.[49] TD-DFT/Tamm-Dancoff approximation (TDA) was also employed to optimize the geometry of the first singlet excited state.[50] The first triplet was optimized from the ground state, from an Unrestricted Kohn Sham for open shell systems calculation with multiplicity equal to three. These geometries were used to calculate the spin-orbit couplings (SOC) between the first five singlet and triplet states. The SOC matrix elements on top of the TD-DFT results were done by using a *quasi*-degenerate perturbation theory.[36,37] SOC integrals are calculated using a mean-field approach named as RI-SOMF (1X) described elsewhere.[51] The calculations also included Grimme's dispersion correction with damping D3BJ[52,53] and the RIJCOSX algorithm was employed to accelerate the evaluation of the integrals, using the resolution of identity approximation for the Coulomb part (RIJ), and the chain of spheres approach for the exchange (COSX).[54,55] RIJCOSX requires the specification of an auxiliary basis set (DEF2/J) for the Coulomb part and a numerical integration grid (GRID/GRIDX5) for the exchange part as discussed elsewhere. The conductor-like polarizable continuum model (CPCM)[56] was employed to account the effect of a solvent with relative permittivity of 37.5 on the electronic structure, corresponding to acetonitrile. The 3D representation of the complexes was obtained using the Chemcraft program.[57]

Results and Discussion

The absorption properties of *fac*-[$Re(CO)_3$(NN)py], NN = phen (**1**), dpq (**2**), and dppz (**3**) in fluid solvents and at room temperature are well described in the literature and do not differ from analog complexes.[58,59] Complexes **1** and **2** are characterized by low energy MLCT bands centered at 370 nm (Figure 1), so the additional pyrazine ring in dpq does not lead to significant shifts on the MLCT band. Only changes in the high energy IL ($\pi \rightarrow \pi^*$) bands are observed. For complex **3**, the MLCT band is overlapped with ligand centered $\pi \rightarrow \pi^*$ transitions, so no shifts are observed in relation to the absorption bands of **1** and **2**, only an increase in the molar absorptivity.

Emission spectra of the investigated complexes in acetonitrile at 298 K are also presented in Figure 1. The emission profiles of **1** and **2** are almost identical. Non-structured broad bands typical of ^{3}MLCT emitters are observed for both complexes, with the emission maximum for **2** ca. 12 nm red-shifted in relation to that observed for **1**. The observed luminescent behavior of both complexes is similar to those previously reported by Wallace and Rillema[60] for **1** and by Lo *et al.*[34] for **2**. Although the emission profile is very similar for both complexes, the substitution of phen by dpq leads to a decrease in the emission quantum yield of ca. 50% (0.020 to 0.012) associated with an expected much shorter emission lifetime (1.6 to 0.45 µs), Table 1. For **3**, a structured emission band is observed at 298 K and is attributed to the triplet intraligand ($^3IL_{dppz}$) radiative decay as also observed for Dyer *et al.*[58]

Table 1 summarizes the luminescent properties of all three investigated complexes in CH_3CN at 298 K.

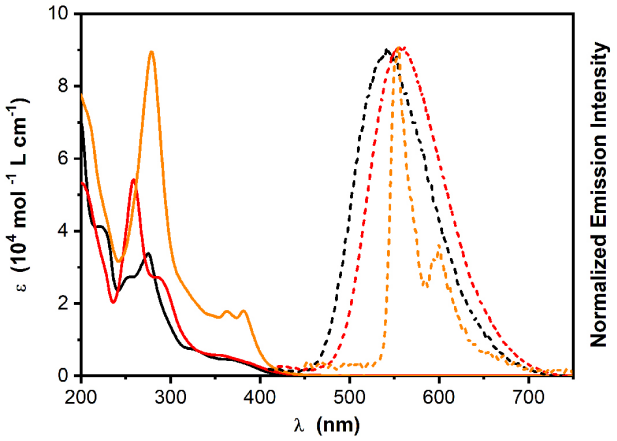

Figure 1. Absorption (solid lines) and emission (dashed lines) spectra of *fac*-[Re(CO)$_3$(NN)(py)]$^+$ in acetonitrile at 298 K. (**1**) Black, (**2**) red and (**3**) orange; λ_{exc} = 375 nm.

Table 1. Photophysical data for the *fac*-[Re(CO)$_3$(NN)(py)]$^+$ in CH_3CN at 298 K (λ_{exc} = 375 nm)

NN	λ_{em} / nm	ϕ	τ / µs
phen (**1**)	545	0.020 ± 0.001	1.6[60]
dpq (**2**)	557	0.012 ± 0.003	0.45[34]
dppz (**3**)	554, 600	0.0010 ± 0.0002	108 ± 10[58]

λ_{em}: emission maxima; ϕ: emission quantum yields; τ: emission lifetime; phen: 1,10-phenanthroline; dpq: dipyrido[3,2-*f*:2',3'-*h*]quinoxaline; dppz: dipyrido[3,2-*a*:2'3'-*c*]phenazine.

As observed in our previous work,[41] when the phen ligand is replaced by dpq, the emission lifetime and yield are drastically reduced, which was associated with the presence of a dark MLCT state centered at π* orbitals in the pyrazine ring, energetically close to the bright MLCT$_{Re\rightarrow phen}$ state. In **3**, the phenazine orbitals are even more stabilized and the luminescent properties are fully dominated by the $^3IL_{dppz}$ excite state. Moreover, for **3**, Dyer *et al.*[58] reported the presence of a close-lying MLCT state in equilibrium with the emissive ligand-centered state, which makes the excited state decay process quite complex.

To clarify the dynamics between emissive and dark triplet states as a function of the polypyridine ligand, temperature-dependent emission studies were carried out in the range of 80 to 300 K. In Figure 2, it is presented the normalized emission spectra of each complex at different temperatures in propionitrile/butyronitrile 5:4 (prop/but 5:4). Similar data were also obtained in ethanol/methanol 4:1 (EtOH/MeOH 4:1), as shown in Figure S1 (Supplementary Information (SI) section). The solvent mixture does not significantly affect the emission maxima or the behavior as a function of the temperature.

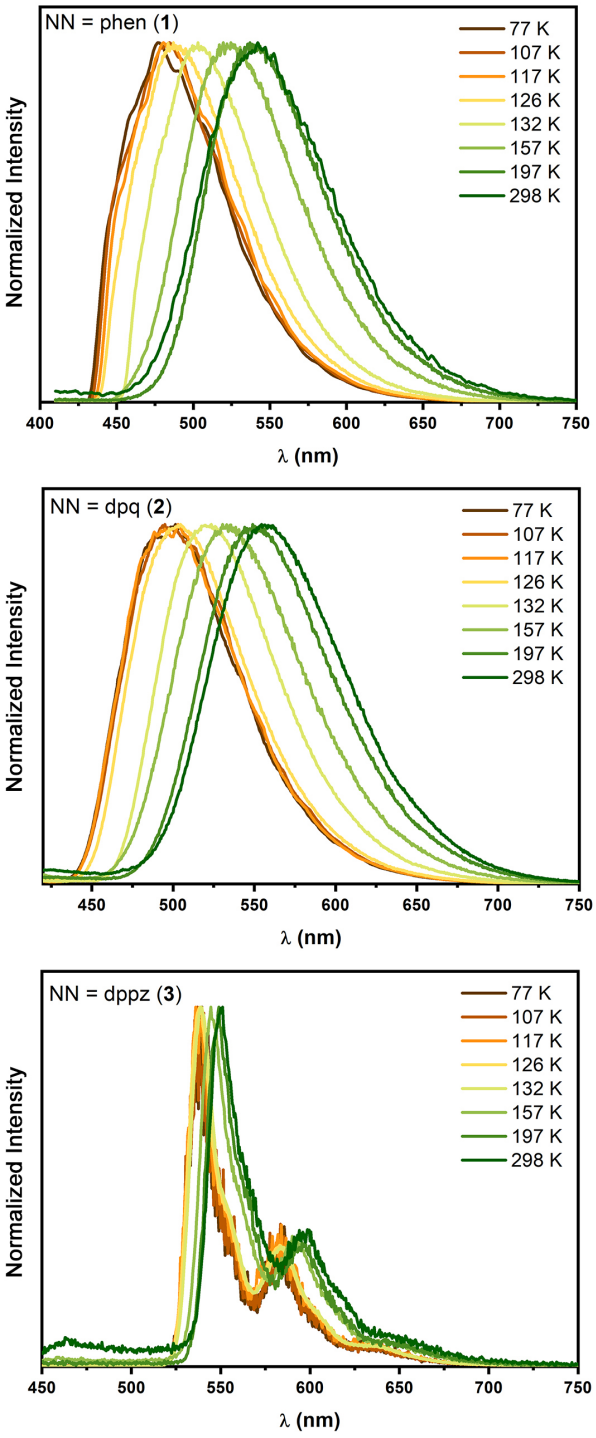

Figure 2. Emission spectra of *fac*-[Re(CO)$_3$(NN)(py)]$^+$ in propionitrile/butyronitrile 5:4 at selected temperatures. λ_{exc} = 375 nm.

As expected for MLCT emitters, complexes **1** and **2** undergo the so-called rigidochromic shift[61,62] in which the energy of the emissive ^{3}MLCT excited state is blue-shifted as the medium rigidity increases. When the ^{3}MLCT excited state is populated, the dipole moment is reversed in comparison to the ground state and the surrounding solvent molecules need to reorient themselves around

the complex to best accommodate the new dipole. This relaxation process takes place readily in fluid solutions at room temperature but is restrained at low temperatures or in rigid media such as polymeric matrices. Consequently, the ^{3}MLCT emitter state is destabilized and blue shifts in the emission maxima are observed. For **3**, the emission maxima are considerably less sensitive to the medium rigidity as the observed luminescence comes from the centrosymmetric $^3IL_{dppz}$ excited state.

Emission quantum yields as a function of the temperature are shown in Figure 3. The values were estimated based on the methodology described by Worl *et al.*[44] and contain uncertainties of ± 20%. As expected, the emission quantum yields decrease as the medium temperature is increased. Complexes **2** and **3** are much more sensitive to temperature than **1**. Despite the quantum yields of all investigated complexes in EtOH/MeOH 4:1 are smaller than those obtained in prop/but 5:4, the behavior as a function of the temperature are very similar in both environments. The quantum yields for **1** are experimentally similar in both solvent mixtures, while for **2** and **3**, smaller values are observed in EtOH/MeOH 4:1, a more polar medium than prop/but 5:4.

To evaluate the expected influence of scattering and major variations of refractive index in frozen media, additional experiments were carried out in an inert polymeric matrix (PMMA). Absorption and emission spectra in this medium are presented in Figures S2 and S3 of the SI section, respectively. No variations are observed in the absorption spectra in relation to those in CH_3CN in accordance with the behavior predicted by the Frank-Condon principle. In the emission spectra however, hypsochromic shifts are observed for **1** and **2** due to the rigidochromic effect. It is important to highlight that the nature of the emission in these complexes remains ^{3}MLCT, even though it can be expected some contribution from upper triplet intraligand states.

The quantum yields were determined against a film containing Rhodamine 6G and are shown in Figure 4. The emission spectra for the standard were also obtained as a function of the temperature and as evidenced from emission spectra in Figure S4, SI section, the areas below the spectra only vary ca. 5% as the temperature goes from 300 to 90 K (at room temperature the emission band is broader as a result of the population of multiple vibronic states). Considering the experimental deviations, one can then consider that the emission quantum yield of Rhodamine 6G in PMMA is independent of the temperature within the investigated range with an average value of 0.72 ± 0.04.

To get further information on the temperature-dependent emission properties of the investigated complexes, the experimental data was modeled as described

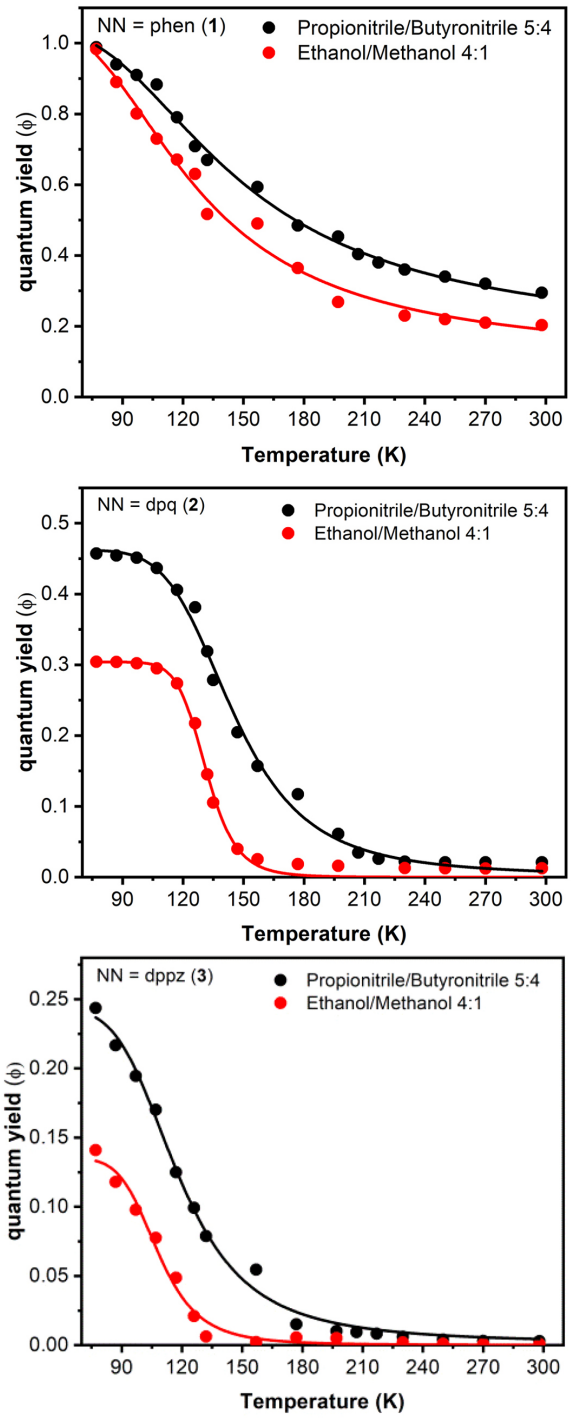

Figure 3. Emission quantum yields of *fac*-$[Re(CO)_3(NN)(py)]^+$ in different solvent mixtures and temperatures. The lines correspond to the fit to a two-level excited state model (refer to the text).

by Wallace *et al.*[63] for **1** and by Hager and Crosby[64] and Meyer and co-workers[65,66] for other polypyridyl metal complexes. The observed behavior can be understood based on a two-level excited state model (Scheme 2), in which the decrease of the observed emission lifetime as a function of the increase in temperature is attributed to the thermal population of a higher-energy non-emitting

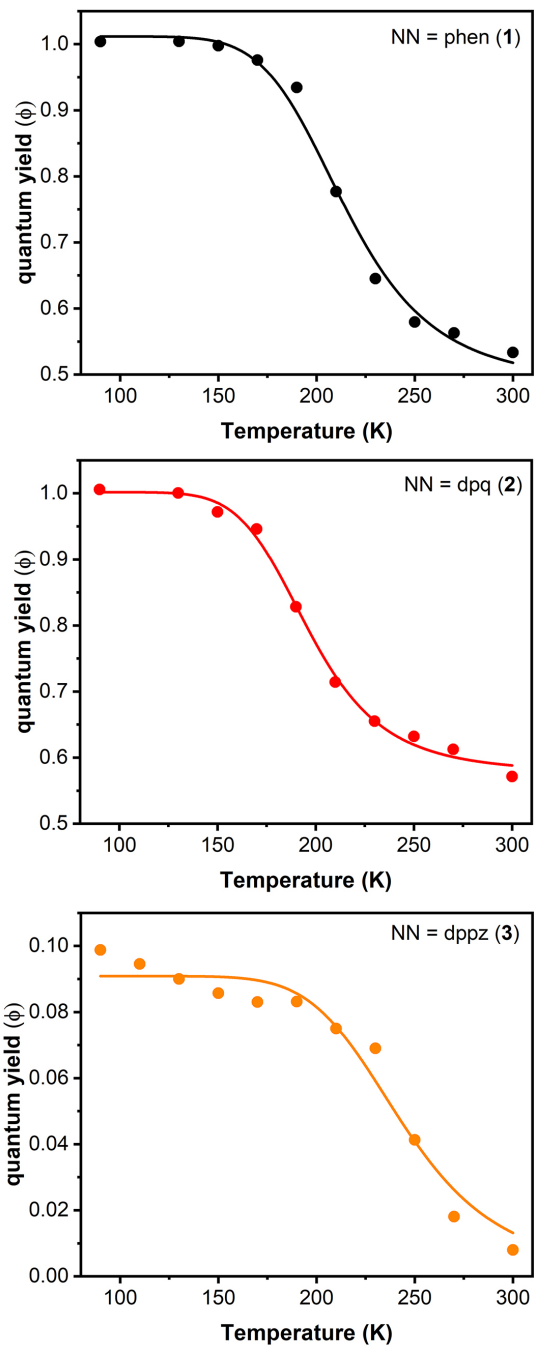

Figure 4. Emission quantum yields of *fac*-[Re(CO)$_3$(NN)(py)]$^+$ in PMMA matrix. The lines correspond to the fit to a two-level excited state model (refer to the text).

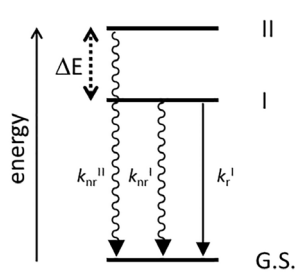

Scheme 2. Two level excited state model used to describe the emission properties as a function of temperature.

excited state (II) with a shorter lifetime than the emitting state (I). For **1**, the energy difference (ΔE) between the emitting ^{3}MLCT state and II obtained by Wallace *et al.*[63] from lifetime measurements in EtOH/MeOH (4:1) was 120 ± 60 cm^{-1}. The nature of II was not elucidated by the authors, although they could exclude the participation of the ligand-centered triplet excited-state, ^{3}LC.

According to the above mentioned model, the emission lifetimes ($\tau = 1/k_{obs}$) can then be fitted by equation 3 in which k_0 is a temperature independent term that accounts for both radiative (k_r^I) and non-radiative (k_{nr}^I) rates from the low-lying excited state and k_1 is the non-radiative rate constant from the upper state (k_{nr}^{II}) that lies at ΔE above the emitting state. In equation 3, T is the temperature, R the ideal gas constant and the denominator $\left[1+\exp\left(-\frac{\Delta E}{RT}\right)\right]$ corrects for electronic distribution between close-lying MLCT states and it is only important when $\Delta E < 3k_BT$ (k_B = Boltzmann constant), which is not the case for the experimental data presented here.

$$k_{obs} = \frac{\left[k_0 + k_1 \exp\left(-\frac{\Delta E}{RT}\right)\right]}{1+\exp\left(-\frac{\Delta E}{RT}\right)} \quad (3)$$

As $\phi = k_r^I/k_{obs}$, equation 3 can be used to fit the experimental data presented in Figures 3 and 4; however, the large number of variables along with the fact that the data is based on steady state measurements lead to rate constant values with very large uncertainties. To overcome such inconvenience, the equation can be rewritten as shown in equation 4, which full mathematical deduction is described in the SI section.

$$\phi = \frac{\phi_I}{1 + A\exp^{\frac{-\Delta E}{RT}}} \quad (4)$$

In equation 4, $\phi_I = \frac{k_r^I}{k_r^I + k_{nr}^I}$ and the pre-exponential term A is defined as $A = \eta_{II}^0 \frac{\left(k_{nr}^{II} + k_{nr}^I\right)}{k_r^I + k_{nr}^I}$, in which η_{II}^0 is the temperature independent term related to fraction of photons that populates the upper state II. The experimental quantum yields in both solvent mixtures and in PMMA were fitted to equation 4 and the fit parameters are presented in Table 2 along with the associated errors. It is worth to note that the values of ΔE obtained by both equations 3 and 4 are numerically similar within a deviation of 5%.

Looking at the fit parameters for the two solvent mixtures, the same values could be used for fitting the data

Table 2. Fit parameters extracted from the temperature-dependent emission lifetimes

Complex	Medium	ΔE / cm^{-1}	A	ϕ_I	R^2
	prop/but 5:4	276 ± 15	10 ± 1	0.99 ± 0.03	0.995
1	EtOH/MeOH 4:1	274 ± 20	18 ± 3	0.99 ± 0.05	0.991
	PMMA	1404 ± 100	$(1.2 \pm 0.8) \times 10^4$	1.00 ± 0.02	0.991
	prop/but 5:4	781 ± 40	$(2 \pm 1) \times 10^3$	0.46 ± 0.01	0.995
2	EtOH/MeOH 4:1	845 ± 60	$(1.1 \pm 0.3) \times 10^4$	0.32 ± 0.01	0.980
	PMMA	1408 ± 100	$(2.9 \pm 0.3) \times 10^4$	1.00 ± 0.02	0.996
	prop/but 5:4	553 ± 45	$(8 \pm 3) \times 10^2$	0.24 ± 0.01	0.994
3	EtOH/MeOH 4:1	562 ± 60	$(2.4 \pm 0.5) \times 10^3$	0.15 ± 0.01	0.970
	PMMA	1643 ± 500	$(1.5 \pm 0.8) \times 10^4$	0.09 ± 0.02	0.970

ΔE: energy difference; A: pre-exponential term of equation 4; ϕ_I: parameter of equation 4; R^2: correlation coeficient for the fitting to equation 4; PMMA: polymethyl methacrylate.

below and above the glass-to-fluid transition temperature in both matrixes, which exhibit different glassy points (ca. 125 K for EtOH:MeOH 4:1; ca. 150 K for prop/but 5:4). This behavior has been observed before for $[Ru(bpy)_3]^{2+}$ in temperature regions, in which the upper lying d-d state is not yet accessible,[67] and for other Re^I tricarbonyl complexes[68] and can be explained by the existence of a single emitting state in the whole temperature range. As the temperature increases, large amplitude (low-frequency) vibrational modes come into play, which enhances the yield of non-radiative deactivation processes.

In PMMA, those low-frequency vibrational modes are inhibited by the matrix itself and as a result, the quantum yields are less dependent on the temperature. Nevertheless, a clear sigmoidal behavior can be observed for **1** and **2** (Figure 4), like those seen in the solvent mixtures (Figure 3). For **3**, this trend is not so clear with the quantum yields being relatively constant from 80 to approximately 200 K and then a sharp decrease is observed up to 300 K. Equation 4 does fit the experimental points, but with poorer correlation coefficient in relation to those for the other complexes. As will be further discussed in the text, the model in Scheme 2 may be not fully appropriate to describe the photophysical behavior of **3**.

We focus our attention now on the main parameter that can be analyzed by the application of equation 4, i.e., the ΔE values. Considering first the solvent mixtures, one can observe that they are independent of the matrix composition and, therefore, related to internal vibrational modes of the respective complexes, rather than to intermolecular interactions with the solvent molecules. It is worth noting that complex **2** exhibits ΔE much higher than **1**. For the latter the value of ΔE lies within the same order of magnitude of the value previous reported.[63] Complex **3** exhibits intermediary values of ΔE in relation to **1** and **2**. In PMMA, ΔE values for all complexes are ca. 10-fold higher, as the vibronic states eventually responsible for the thermal population of the upper dark excited state (II) are not accessible.

In order to get further insights on the nature of II and its temperature-dependent population in the investigated complexes, the optimized geometries for the ground state, S_1, T_1, T_2 and T_3 excited states of all complexes were obtained by TD-DFT. The predicted S_0 geometry for all complexes are in good agreement with single crystal data,[10,33] where the maximum average error found for bond lengths were of 4.60%, and 3.92% for bond angles, which supports the further use of PBE0 in subsequent investigations. Then, spin-orbit coupling (SOC) matrix elements between the first 5 singlet and triplet states were calculated on top of the S_1 geometry. The energies of these states and the SOC matrix elements obtained between the triplet states and the first excited singlet state are shown in Table 3. The SOC matrix elements can be interpreted based on the orthogonality of the involved states and their spatial distance: a large SOC matrix element is expected for states with high orthogonality (distinct excited state configuration), close energies and high contribution of the metal center that has a high spin-orbit coupling constant.

Isosurface plots of the frontier orbitals of the complexes are presented in Figure S5, SI section. Based on the calculated energies shown in Table 3, a simplified energy diagram of the lowest lying singlet and triplet states can be drawn, Figure 5.

The direct intersystem crossing from S_1 to T_1 is unlikely for all investigated complexes since low SOC matrix elements were obtained between such states. This is expected since S_1 and T_1 have very similar configurations and therefore low orthogonality among themselves. In all complexes, the lowest lying singlet and triplet states are MLCT in nature, with electrons being transferred from d orbitals in Re^I center to π* orbitals of phenanthroline aromatic rings (see Figure 4). Particularly for **3**, one can observe that in the first three low lying triplet states the

Table 3. SOC-TD-DFT data for the investigated rhenium(I) complexes

State	Energy / eV	$\langle S_i\|H_{SO}\|T_n\rangle^a$ / cm^{-1}	Contribution^b / %	Attribution
fac-[Re(CO)$_3$(phen)(py)]$^+$ (**1**)				
S_1	2.30^c	–	H → L (98)	^{1}MLCT
S_2	2.99^d	–	H → L+1 (41) H-1 → L (50)	^{1}MLCT ^{1}MLCT
T_1	1.96^c	20	H → L (89)	^{3}MLCT
T_2	2.24^c	623	H-1 → L (86)	^{3}MLCT
T_3	2.42^c	970	H-2 → L (94)	^{3}MLCT
fac-[Re(CO)$_3$(dpq)(py)]$^+$ (**2**)				
S_1	2.20^c		H → L (98)	^{1}MLCT
S_2	2.82^d		H → L+1 (96)	^{1}MLCT
T_1	1.80^c	27	H → L (93)	^{3}MLCT
T_2	2.22^c	717	H-1 → L (93)	^{3}MLCT
T_3	2.27^c	953	H-2 → L (97)	^{3}MLCT
fac-[Re(CO)$_3$(dppz)(py)]$^+$ (**3**)				
S_1	2.16^c	–	H → L (60) H → L+1 (38)	^{1}MLCT ^{1}MLCT
S_2	2.49^d	–	H → L (39) H → L+1 (60)	^{1}MLCT ^{1}MLCT
T_1	1.79^c	23	H → L (39) H-1 → L (53)	^{3}MLCT ^{3}MLCT
T_2	2.13^c	18	H-5 → L (91)	^{3}ILCT
T_3	2.24^c	726	H-4 → L (51) H-2 → L (42)	^{3}ILCT ^{3}MLCT

$^a\sqrt{\sum\alpha} = x, y, z\ (\langle S_i|H_{SO}|T_{j,\alpha}\rangle)^2$ at the S_1 optimized geometry; ^{b}transitions with high percentage (> 10%) contributions are shown in parenthesis; ^{c}adiabatic energy; ^{d}vertical SOC-TD-DFT energy at the S_0 optimized geometry. MLCT: metal-to-ligand charge transfer; ILCT: intraligand charge transfer.

charge is transferred to the π* orbitals of phenazine moiety in the dppz ligand, which are poorly emissive. The ascribed emitting states at room temperature and fluid media are T_1 for complexes **1** and **2**, and T_2 for **3**. Such attribution is made based on the nature of the triplet states and the observed experimental data, i.e., broad band long-lived ^{3}MLCT emissions for **1** and **2** with moderated quantum yields and structured long-lived ^{3}IL band for **3** with much smaller quantum efficiency.

Both experimental and theoretical data indicate that the emissive lowest lying triplet state is stabilized as the phen ligand in **1** is replaced by dpq in **2**. The observed red-shift in the emission maxima was 12 nm, corresponding to an energy variation of 0.05 eV, while the calculated difference was 0.16 eV. In both complexes, the population of T_1 occurs through internal conversion from an upper triplet state with a higher SOC matrix element with S_1. For **1** and **2**, the SOC matrix element between S_1 and T_2 is considerably high, indicating a high probability of the intersystem to occur between them. In **1**, T_2 is lower in energy than S_1 by 0.06 eV or 484 cm^{-1} and the SOC matrix element between these states is 623 cm^{-1}. This indicates a high coupling between these two states with fast interconversion to the emitting T_1 state. In fact, at frozen media, the observed quantum yield is nearly 100% and after the glass-to-fluid transition, the fraction of radiative decay remains higher than that observed in **2**, despite the activation energy to populate vibronic states of upper states (either S_1 or T_2) is less than half than that observed for **2**.

In **2**, the intersystem crossing from S_1 occurs preferentially to T_2 that lies ca. 0.02 eV or 160 cm^{-1} above S_1. As a consequence, the phosphorescence quantum yield in **2** is 50-70% smaller than **1** in frozen media depending on the solvent employed. In a more polar medium, such as EtOH:MeOH 4:1 mixtures, the quantum yields at low temperature are considerably lower than in prop/but 5:4, which indicates the contribution of low-frequency vibration modes involving the first solvation layer to the energy dissipation.

In fluid media, the stabilization of the emissive T_1 state in relation to its counterpart in **1** also disfavors the radiative decay as predicted by the golden rule.[69] The higher activation

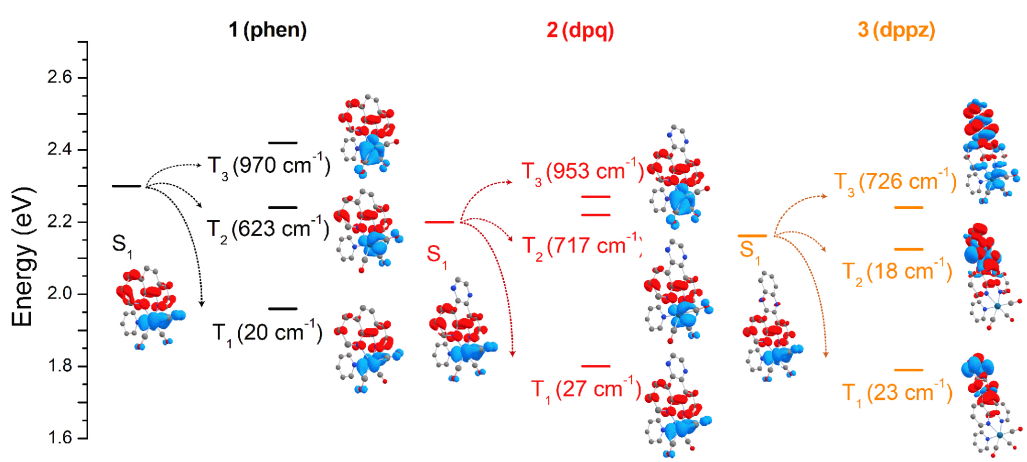

Figure 5. Excited state energy diagram of the investigated *fac*-[Re(CO)$_3$(NN)(py)] complexes based on SOC-TD-DFT calculations. The spin-orbit coupling matrix (SOCME) element values in parenthesis were calculated using $\sqrt{\sum\alpha} = x, y, z\ (\langle S_i|H_{SO}|T_{j,\alpha}\rangle)^2$. Figures in each state correspond to the variation of the electron density in relation to the respective ground states.

energy found for **2** is an indication of low coupling between T_1 and the upper excited states (S_1 or T_2) which would also favors the non-radiative decay from these states directly to the ground state. In fact, direct relaxation from the lowest lying singlet state (fluorescence) or upper triplet states has been reported to *fac*-[$Re(CO)_3$(bpy)(L)] complexes, bpy = 2,2'-bipirydine.[70] The authors found out that the intersystem crossing rates here are surprisingly slower than those for Ru^{II} or Fe^{II} bipyridine complexes despite the high SOC constant of the Re^{I} center, and they are highly dependent on the coordination environment. SOC-TD-DFT calculations indicate that the intersystem crossing from the S_1 zeroth vibrational level to T_2 in **2** is energetically disfavored compared to **1** and **3**, thus one can expect a higher contribution of direct relaxation from S_1 to the ground state.

Based on the theoretical calculations, the nature of the higher-energy non-emitting excited state II is likely to be T_2 for **1** and the singlet lowest lying MLCT state S_1 for **2**. In **1**, T_2 is closer in energy to T_1 in relation to what is observed in **2**. As result, smaller activation energies are required to thermally populate it, but the overall quantum yield for **1** remains higher due the fast interconversion between these two triplet states. For **2**, on the other hand, there is a lower coupling between the emitting T_1 state and the upper lying excited states. Thus, once there is enough thermal energy to populate T_2 or S_1, the radiative decay from T_1 is partially hindered by direct decay from S_1, which is slightly more stabilized than T_2.

In PMMA matrix the differences observed between **1** and **2** in the solvent mixtures practically disappear. In this more rigid medium, both the absorption and emission maxima of the two complexes are close in energy and the population of multiple vibronic states of T_1 and S_1 is hindered even at room temperature, so the differences in the population of upper-lying excited states observed in fluid solution tend to be minimized. Moreover, due to the rigidochromic effect, the triplet states are destabilized, while the singlet states remain unaltered. Thus, we can also expect that the intersystem crossing from S_1 to T_2 should be uphill in both cases. All these factors lead to very similar photophysical behavior between these complexes in PMMA matrix.

Complex **3** exhibits a more complex photophysical behavior. Its calculated energy diagram and the photophysical parameters agree well with those previously reported by Dyer *et al.*[58] The emissive ligand-centered triplet state (T_2) is not the lowest lying excited state, one of the assumptions of the three-state model used to fit the experimental data. As the radiative decay does not occur from the lowest lying triplet state, in the fluid medium the emission quantum yields are nearly zero, due to the internal conversion to T_1.

T_1 and T_3 are MLCT in nature but the charge is transferred from the metal to the phenazine moiety of dppz, leading to very weak emissive properties, compared to the population of the phenanthroline π* orbitals. Moreover, the intersystem crossing from S_1 occurs preferentially to T_3, which lies 0.08 eV or 640 cm^{-1} uphill. So, in fact, for **3**, k_{nr}^{I} that appears on the Scheme 2 is the internal conversion from T_2 to the lower-energy triplet T_1, which is must faster than k_r^{I} and leads to the much more abrupt variation observed in the quantum yields as a function of the temperature. In more constrained media, the interconversion from T_2 to T_1 is inhibited leading to higher quantum yields. As the temperature is increased to 180-200 K, the internal conversion is triggered leading to the quenching of the intraligand phosphorescence. Previous time-resolved infrared studies[58] reveal a poor coupling between T_1 and the ground state, favoring the observation of the weak phosphorescence from T_2. The same dependence on the polarity of the solvent observed for **2** occurs for **3**, i.e., the more polar is the medium, lower is the quantum yield.

One important insight not reported before for **3** is related to the intersystem crossing process. The calculated SOC matrix elements reveal that the intersystem crossing (ISC) pathway between the emissive T_2 state and S_1 is less favorable than the most likely ISC from S_1 to the T_3 state, 0.08 eV (640 cm^{-1}) uphill. This is a considerable energy barrier that should favor singlet deactivation pathways from S_1. The population of T_2 should probably occur through upper lying singlet states of intraligand character. The ΔE values obtained in solvent mixtures match well with the energy difference between T_3 and S_1, although the results are not conclusive given the clear role of at least five different states (S_0, S_1, T_1, T_2, and T_3) to the photophysical properties. Nevertheless, the results found for **3** agree with the observed behavior of this compound as a luminescent DNA sensor. Light-excitation after the interaction with the biomolecule leads to two different phenomena:[27,30,71] enhancement of the ^{3}IL phosphorescence, resulting from the inhibition of the energy dissipation through the low frequency vibrational modes, and oxidation of DNA, as a result of the population of long-lived dark MLCT states.

In **2**, TD-DFT calculations indicate that the unoccupied π* molecular orbitals centered at the pyrazine ring (LUMO+1) do not contribute significantly to the lowest lying triplet states. Possible interaction of **2** with electron-withdrawing species or either with more polar solvent molecules can lead to stabilization of such orbitals triggering new intersystem crossing pathways. This strategy can be further used for sensing applications as shown by Lo *et al.*[33-35] for related complexes. The authors have shown that the emission quantum yields of

fac-[Re(CO)$_3$(dpq)(L)]$^+$ are improved in non-polar solvents which agree well with our findings.

Conclusions

The temperature-dependent emission properties of a series of *fac*-[Re(CO)$_3$(NN)(py)]$^+$, NN = phen (**1**), dpq (**2**), and dppz (**3**), were investigated and rationalized based on TD-DFT calculations, including for the first time for this class of compounds the determination of SOC matrix elements. The photophysical behavior in fluid and rigid medium has been fully unveiled as a function of the excited state dynamics with the determination of the main intersystem crossing pathways as well as the activation energies associated with thermal population of non-emitting upper states. The nature of these upper states have also been ascribed for the first time, while for complex **3**, these properties have been largely explored for DNA probing, the possible sensing applications of **2** and its analogs are still poorly investigated. Its emission quantum yield is smaller than **1** in fluid solvents but much larger than **3**, keeping the dependence on the medium polarity and intermolecular interactions. Therefore, it can be further explored as a sensor with improved limits of detection.

Supplementary Information

Supplementary information (mathematical deduction of equation 4, along with additional photophysical data and isosurface plots of selected frontier molecular orbitals of the investigated Re^{I} complexes) is available free of charge at http://jbcs.sbq.org.br as PDF file.

Acknowledgments

This work was supported by Fundação de Amparo à Pesquisa do Estado de Minas Gerais (FAPEMIG, PPM-00220-17), Conselho Nacional de Desenvolvimento Científico e Tecnológico (CNPq, 406392/2018-8, 310303/2018-4) and Coordenação de Aperfeiçoamento de Pessoal de Nível Superior (CAPES). The authors are also thankful to the Grupo de Materiais Inorgânicos do Triângulo (GMIT), a research group supported by FAPEMIG (APQ-00330-14). A.O.T.P. is thankful to Alexander von Humboldt Foundation for the financial support.

Author Contributions

C.L.R., F.S.P. and M.E.G.C. performed the synthesis and characterization of the complexes as well as the photophysical experiments; G.F., B.S. and A.E.H.M. have performed the quantum-mechanical calculation, their validation and have greatly contributed for the interpretation of the experimental results; A.O.T.P. was responsible for the conceptualization, funding acquisition, writing and review.

References

1. Atallah, H.; Taliaferro, C. M.; Wells, K. A.; Castellano, F. N.; *Dalton Trans.* **2020**, *49*, 11565.
2. Rohacova, J.; Ishitani, O.; *Dalton Trans.* **2017**, *46*, 8899.
3. Mizoguchi, S. K.; Patrocinio, A. O. T.; Iha, N. Y. M.; *Synth. Met.* **2009**, *159*, 2315.
4. Barnsley, J. E.; Shillito, G. E.; Larsen, C. B.; van der Salm, H.; Horvath, R.; Sun, X. Z.; Wu, X.; George, M. W.; Lucas, N. T.; Gordon, K. C.; *Inorg. Chem.* **2019**, *58*, 9785.
5. Faustino, L. A.; Souza, B. L.; Nunes, B. N.; Duong, A. T.; Sieland, F.; Bahnemann, D. W.; Patrocinio, A. O. T.; *ACS Sustainable Chem. Eng.* **2018**, *6*, 6073.
6. Faustino, L. A.; Machado, A. E. H.; Patrocinio, A. O. T.; *Inorg. Chem.* **2018**, *57*, 2933.
7. Chen, H.; Zhang, Y. J.; Bonfiglio, A.; Morlet-Savary, F.; Mauro, M.; Lalevee, J.; *ACS Appl. Polym. Mater.* **2021**, *3*, 464.
8. Nguyen, M. T.; Jones, R. A.; Holliday, B. J.; *Coord. Chem. Rev.* **2018**, *377*, 237.
9. Carreno, A.; Paez-Hernandez, D.; Zuniga, C.; Ramirez-Osorio, A.; Pizarro, N.; Vega, A.; Solis-Cespedes, E.; Rivera-Zaldivar, M. M.; Silva, A.; Fuentes, J. A.; *Dyes Pigm.* **2021**, *184*, 108876.
10. Murphy, B. L.; Marker, S. C.; Lambert, V. J.; Woods, J. J.; MacMillan, S. N.; Wilson, J. J.; *J. Organomet. Chem.* **2020**, *907*, 121064.
11. Zhang, K. Y.; Yu, Q.; Wei, H. J.; Liu, S. J.; Zhao, Q.; Huang, W.; *Chem. Rev.* **2018**, *118*, 1770.
12. Lo, K. K. W.; *Acc. Chem. Res.* **2015**, *48*, 2985.
13. Valdes, E.; Cepeda-Plaza, M.; Gunther, G.; Vega, A.; Palacios, R.; Gomez, M. L.; Pizarro, N.; *Dyes Pigm.* **2020**, *172*, 107787.
14. Shillito, G. E.; Preston, D.; Traber, P.; Steinmetzer, J.; McAdam, C. J.; Crowley, J. D.; Wagner, P.; Kupfer, S.; Gordon, K. C.; *Inorg. Chem.* **2020**, *59*, 6736.
15. Yip, A. M. H.; Shum, J.; Liu, H. W.; Zhou, H. P.; Jia, M. Q.; Niu, N.; Li, Y. X.; Yu, C.; Lo, K. K. W.; *Chem.- Eur. J.* **2019**, *25*, 8970.
16. Sato, S.; McNicholas, B. J.; Grubbs, R. H.; *Chem. Commun.* **2020**, *56*, 4440.
17. Fantini, G.; Dallerba, E.; Massi, M.; Lowe, A. B.; *Macromol. Chem. Phys.* **2020**, *221*, 2000135.
18. Liang, H. P.; Acharjya, A.; Anito, D. A.; Vogl, S.; Wang, T. X.; Thomas, A.; Han, B. H.; *ACS Catal.* **2019**, *9*, 3959.
19. Sathish, V.; Krishnan, M. M.; Velayudham, M.; Thanasekaran, P.; Lu, K. L.; Rajagopal, S.; *Spectrochim. Acta, Part A* **2019**, *222*, 117160.

20. Zhao, G. W.; Zhao, J. H.; Hu, Y. X.; Zhang, D. Y.; Li, X.; *Synth. Met.* **2016**, *212*, 131.
21. Goncalves, M. R.; Benvenho, A. R. V.; Frin, K. P. M.; *Opt. Mater.* **2019**, *94*, 206.
22. Pizl, M.; Picchiotti, A.; Rebarz, M.; Lenngren, N.; Liu, Y. L.; Zalis, S.; Kloz, M.; Vlcek, A.; *J. Phys. Chem. A* **2020**, *124*, 1253.
23. Cheng, S. C.; Chu, W. K.; Ko, C. C.; Phillips, D. L.; *ChemPhysChem* **2019**, *20*, 1946.
24. Mai, S.; Gattuso, H.; Fumanal, M.; Munoz-Losa, A.; Monari, A.; Daniel, C.; Gonzalez, L.; *Phys. Chem. Chem. Phys.* **2017**, *19*, 27240.
25. Gourlaouen, C.; Eng, J.; Otsuka, M.; Gindensperger, E.; Daniel, C.; *J. Chem. Theory Comput.* **2015**, *11*, 99.
26. Coogan, M. P.; Platts, J. A.; *Chem. Comm.* **2016**, *52*, 12498.
27. Alberti, E.; Coogan, M. P.; Donghi, D.; *J. Biol. Inorg. Chem.* **2014**, *19*, S824.
28. Thorp-Greenwood, F. L.; Coogan, M. P.; Mishra, L.; Kumari, N.; Rai, G.; Saripella, S.; *New J. Chem.* **2012**, *36*, 64.
29. Smith, J. A.; George, M. W.; Kelly, J. M.; *Coord. Chem. Rev.* **2011**, *255*, 2666.
30. Creely, C. M.; Kelly, J. M.; Feeney, M. M.; Hudson, S.; Penedo, J. C.; Blau, W. J.; Elias, B.; Kirsch-De Mesmaeker, A.; Matousek, P.; Towrie, M.; Parker, A. W.; Dyer, J. S.; George, M. W.; Coates, C. G.; Mc Garvey, J. J. In *Opto-Ireland 2002: Optics and Photonics Technologies and Applications, Pts 1 and 2*, vol. 4876; Blau, W. J.; Donegan, J. F.; Duke, A. F.; MacCraith, J. A.; McMillan, N. D.; Oconnor, G. M.; Omongain, E.; Toal, V.; McLaughlin, J. A., eds.; Society of Photo Optical: Washington, USA, 2003.
31. Moncada, A. S.; Gutierrez-Pineda, E.; Maisuls, I.; Ruiz, G. T.; Lappin, A. G.; Ferraudi, G. J.; Wolcan, E.; *J. Photochem. Photobiol., A* **2018**, *353*, 86.
32. Summers, P. A.; Calladine, J. A.; Ibrahim, N.; Kusumo, K. P.; Clark, C. A.; Sun, X. Z.; Hamilton, M. L.; Towrie, M.; McMaster, J.; Schroder, M.; George, M. W.; *Polyhedron* **2017**, *123*, 259.
33. Lo, K. K. W.; Sze, K. S.; Tsang, K. H. K.; Zhu, N. Y.; *Organometallics* **2007**, *26*, 3440.
34. Lo, K. K.-W.; Tsang, K. H.-K.; Sze, K.-S.; *Inorg. Chem.* **2006**, *45*, 1714.
35. Lo, K. K. W.; Hui, W. K.; *Inorg. Chem.* **2005**, *44*, 1992.
36. de Souza, B.; Farias, G.; Neese, F.; Izsák, R.; *J. Chem. Theory Comput.* **2019**, *15*, 1896.
37. de Souza, B.; Neese, F.; Izsák, R.; *J. Chem. Phys.* **2018**, *148*, 034104.
38. Dickeson, J. E.; Summers, L. A.; *Aust. J. Chem.* **1970**, *23*, 1023.
39. Yamada, M.; Tanaka, Y.; Yoshimoto, Y.; Kuroda, S.; Shimao, I.; *Bull. Chem. Soc. Jpn.* **1992**, *65*, 1006.
40. Arias, M.; Concepcion, J.; Crivelli, I.; Delgadillo, A.; Diaz, R.; Francois, A.; Gajardo, F.; Lopez, R.; Leiva, A. M.; Loeb, B.; *Chem. Phys.* **2006**, *326*, 54.
41. Sousa, S. F.; Sampaio, R. N.; Neto, N. M. B.; Machado, A. E. H.; Patrocinio, A. O. T.; *Photochem. Photobiol. Sci.* **2014**, *13*, 1213.
42. Patrocinio, A. O. T.; Brennaman, M. K.; Meyer, T. J.; Iha, N. Y. M.; *J. Phys. Chem. A* **2010**, *114*, 12129.
43. Nunes, B. N.; Lopes, O. F.; Patrocinio, A. O. T.; Bahnemann, D. W.; *Catalysts* **2020**, *10*, 126.
44. Worl, L. A.; Duesing, R.; Chen, P. Y.; Dellaciana, L.; Meyer, T. J.; *J. Chem. Soc., Dalton Trans.* **1991**, 849.
45. Nunes, B. N.; Patrocinio, A. O. T.; Bahnemann, D. W.; *J. Phys.: Condens. Matter* **2019**, *31*, 394001.
46. Neese, F.; *WIREs Comput. Mol. Biosci.* **2018**, *8*, e1327.
47. Perdew, J. P.; Burke, K.; Ernzerhof, M.; *Phys. Rev. Lett.* **1996**, *77*, 3865.
48. Perdew, J. P.; Burke, K.; Ernzerhof, M.; *Phys. Rev. Lett.* **1997**, *78*, 1396.
49. Pantazis, D. A.; Chen, X.-Y.; Landis, C. R.; Neese, F.; *J. Chem. Theory Comput.* **2008**, *4*, 908.
50. Petrenko, T.; Kossmann, S.; Neese, F.; *J. Chem. Phys.* **2011**, *134*, 054116.
51. Neese, F.; *J. Chem. Phys.* **2005**, *122*, 034107.
52. Grimme, S.; Antony, J.; Ehrlich, S.; Krieg, H.; *J. Chem. Phys.* **2010**, *132*, 154104.
53. Grimme, S.; Ehrlich, S.; Goerigk, L.; *J. Comput. Chem.* **2011**, *32*, 1456.
54. Izsák, R.; Neese, F.; *J. Chem. Phys.* **2011**, *135*, 144105.
55. Izsák, R.; Neese, F.; Klopper, W.; *J. Chem. Phys.* **2013**, *139*, 094111.
56. Marenich, A. V.; Cramer, C. J.; Truhlar, D. G.; *J. Phys. Chem. B* **2009**, *113*, 6378.
57. *Chemcraft*, version b610b; Chemcraft, New York, USA, 2019.
58. Dyer, J.; Blau, W. J.; Coates, C. G.; Creely, C. M.; Gavey, J. D.; George, M. W.; Grills, D. C.; Hudson, S.; Kelly, J. M.; Matousek, P.; McGarvey, J. J.; McMaster, J.; Parker, A. W.; Towrie, M.; Weinstein, J. A.; *Photochem. Photobiol. Sci.* **2003**, *2*, 542.
59. Fredericks, S. M.; Luong, J. C.; Wrighton, M. S.; *J. Am. Chem. Soc.* **1979**, *101*, 7415.
60. Wallace, L.; Rillema, D. P.; *Inorg. Chem.* **1993**, *32*, 3836.
61. Patrocinio, A. O. T.; Iha, N. Y. M.; *Inorg. Chem.* **2008**, *47*, 10851.
62. Polo, A. S.; Itokazu, M. K.; Frin, K. M.; Patrocinio, A. O. D.; Iha, N. Y. M.; *Coord. Chem. Rev.* **2006**, *250*, 1669.
63. Wallace, L.; Jackman, D. C.; Rillema, D. P.; Merkert, J. W.; *Inorg. Chem.* **1995**, *34*, 5210.
64. Hager, G. D.; Crosby, G. A.; *J. Am. Chem. Soc.* **1975**, *97*, 7031.
65. Caspar, J. V.; Meyer, T. J.; *J. Am. Chem. Soc.* **1983**, *105*, 5583.
66. Durham, B.; Caspar, J. V.; Nagle, J. K.; Meyer, T. J.; *J. Am. Chem. Soc.* **1982**, *104*, 4803.
67. Barigelletti, F.; Juris, A.; Balzani, V.; Belser, P.; Von Zelewsky, A.; *J. Phys. Chem.* **1986**, *90*, 5190.

68. Ferraudi, G.; Feliz, M.; Wolcan, E.; Hsu, I.; Moya, S. A.; Guerrero, J.; *J. Phys. Chem.* **1995**, *99*, 4929.
69. Claude, J. P.; Meyer, T. J.; *J. Phys. Chem.* **1995**, *99*, 51.
70. Cannizzo, A.; Blanco-Rodríguez, A. M.; El Nahhas, A.; Šebera, J.; Záliš, S.; Vlček, A.; Chergui, M.; *J. Am. Chem. Soc.* **2008**, *130*, 8967.
71. Cao, Q.; Creely, C. M.; Davies, E. S.; Dyer, J.; Easun, T. L.; Grills, D. C.; McGovern, D. A.; McMaster, J.; Pitchford, J.; Smith, J. A.; Sun, X. Z.; Kelly, J. M.; George, M. W.; *Photochem. Photobiol. Sci.* **2011**, *10*, 1355.

Submitted: August 15, 2021
Published online: November 30, 2021

This is an open-access article distributed under the terms of the Creative Commons Attribution License.